Progress In Electromagnetics Research B, Vol. 23, 181–197, 2010

CELL-VERTEX BASED MULTIGRID SOLUTION OF THE TIME DOMAIN MAXWELL'S EQUATIONS

N. Deore and A. Chatterjee

Department of Aerospace Engineering
Indian Institute of Technology Bombay
Mumbai 400 076, India

Abstract—The time domain Maxwell's equations are numerically solved using a multigrid method in a scattered field formulation and a cell-vertex based finite volume time domain framework. The multilevel method is an adaptation of Ni's [9] cell-vertex based multigrid technique, proposed for accelerating steady state convergence of nonlinear Euler equations of gas dynamics. Accelerated convergence to steady state of the time domain Maxwell's equations, for problems involving electromagnetic scattering, is obtained using multiple grids without the use of additional numerical damping usually required in nonlinear problems. The linear nature of the Maxwell's system also allows for a more accurate representation of the fine-grid problem on the coarse grid.

1. INTRODUCTION

Finite volume time domain (FVTD) methods are used to solve the time domain Maxwell's equations written as a system of hyperbolic conservation laws [1–3]. Electromagnetic scattering involving complex geometries, broad-band signals and diverse material properties can be dealt with advantageously using FVTD methods [2, 4]. However, FVTD methods are of limited applicability in predicting electromagnetic scattering for practical applications involving large electric sizes. The computational grid for FVTD methods can be based on resolution of 12–20 points per wavelength (PPW) resulting in very fine meshes at large electrical sizes. This consequently results in long computational times for problems involving large electrical sizes making FVTD techniques prohibitively expensive for many

Received 20 June 2010, Accepted 13 July 2010, Scheduled 22 July 2010
Corresponding author: N. Deore (narendra@aero.iitb.ac.in).

engineering applications. A variety of techniques can be used to bring down computing costs including parallel computing, hybrid methods by combining two or more approaches, incorporating algorithmic acceleration devices like multigrid methods etc. In this work, we use a cell-vertex based multigrid approach to accelerate the convergence to time-harmonic steady state of the time domain Maxwell's equations for electromagnetic scattering problems. The multigrid technique was originally developed for the numerical solution of linear elliptic partial differential equations (PDE) and proved very successful in accelerating the convergence of boundary value problems [6, 7]. The extension of this technique to accelerate the convergence of the solution of hyperbolic PDEs is nontrivial [8]. Hyperbolic PDEs differs from elliptic PDEs in the nature of the solution, and the manner in which the boundary effects the solution. The wave nature of the hyperbolic system lead to numerical schemes with a bias in the direction of propagation. The numerical solution of hyperbolic PDEs can also be advanced to a steady state via multigrid methods by cycling the solution through a hierarchy of fine and coarse grids. In case of hyperbolic equations, accelerated convergence through multigrid methods is achieved due to faster wave propagation on coarser levels due to a more relaxed stability criteria and a sparser grid. Multigrid techniques were extended to the system of hyperbolic equations in the work of Ni [9] and Jameson [10] by exploiting faster wave propagation in the computational domain using coarser grids while solving for the time dependant Euler equations of gas dynamics. However, they relied on heavy user defined numerical damping to stabilize the multigrid scheme and smoothen interpolation errors. In this current work, the multilevel method of Ni [9] is extended to the numerical solution of the time dependant Maxwell's equations for electromagnetic scattering problems. Inherent advantages of applying Ni's cell-vertex based multilevel technique to a linear system of equations compared to the nonlinear Euler equations are brought out along with practical implementation details.

2. GOVERNING EQUATIONS

Maxwell's curl equations in differential form for wave propagation in free space, can be expressed as

$$\frac{\partial \mathbf{B}}{\partial t} + \nabla \times \mathbf{E} = 0 \tag{1}$$

$$\frac{\partial \mathbf{D}}{\partial t} - \nabla \times \mathbf{H} = 0 \tag{2}$$

where **B** is the magnetic induction, **E** the electric field vector, **D** the electric field displacement, and **H** the magnetic field vector. The **B** and **D** are related to **E** and **H** through permittivity (ϵ) and the permeability (μ) with $\mathbf{D} = \varepsilon\mathbf{E}$, and $\mathbf{B} = \mu\mathbf{H}$. The time domain Maxwell's equations can be recast in conservation total field form as

$$\frac{\partial \mathbf{u}}{\partial t} + \frac{\partial \mathbf{f}(\mathbf{u})}{\partial x} + \frac{\partial \mathbf{g}(\mathbf{u})}{\partial y} + \frac{\partial \mathbf{h}(\mathbf{u})}{\partial z} = 0. \tag{3}$$

In two dimensions (2D), Maxwell's equations can be split into two sets of systems. These are the equations for Transverse Magnetic (TM) and Transverse Electric (TE) waves. The 2-D conservative form for free space can be expressed as

$$\frac{\partial \mathbf{u}}{\partial t} + \frac{\partial \mathbf{f}(\mathbf{u})}{\partial x} + \frac{\partial \mathbf{g}(\mathbf{u})}{\partial y} = 0. \tag{4}$$

For TM polarized incident plane wave, the vectors **u**, **f**, and **g** in Equation (4) are

$$\mathbf{u} = \begin{pmatrix} B_x \\ B_y \\ D_z \end{pmatrix}, \quad \mathbf{f} = \begin{pmatrix} 0 \\ -D_z/\epsilon \\ -B_y/\mu \end{pmatrix}, \quad \mathbf{g} = \begin{pmatrix} D_z/\epsilon \\ 0 \\ B_x/\mu \end{pmatrix}. \tag{5}$$

The FVTD technique numerically solves the integral form of Equations (3) or (4) in a discrete finite volume framework and is described in detail in Refs. [1–4, 11]. In a scattered field formulation, the scattered field variables are solved for and an analytically defined incident field assumed to be available, as also described in Refs. [1–4, 11].

3. NUMERICAL SCHEME

The underlying scheme in this current work, for numerically solving the time domain Maxwell's equations, is the cell vertex based finite volume scheme originally proposed by Ni [9] for the numerical solution of the 2D Euler equations of gas dynamics. Details regarding an extension of Ni's cell vertex finite volume scheme to the solution of the time domain Maxwell's equations in scattered field formulation in two and three dimensions were presented in Ref. [11] and is discussed here briefly. Ni's cell-vertex based finite volume scheme can be considered to belong to the "fluctuation-signal" framework proposed by Roe for the solution of time dependant Euler equations of gas dynamics [14]. In Ni's finite-volume time integration scheme, the fluctuation is calculated based on state vector stored at cell vertices and distributed to cell vertices after a discrete time-step. This distribution finally leads to second-order accurate cell-vertex based Lax-Wendroff scheme [15]. Ni, in his original

paper, required heavy numerical damping while solving for strongly nonlinear systems encountered in the form of transonic flows in gas dynamics. The linear nature of the time dependant Maxwell's equation in free space, may be a more appropriate choice for the application of Ni's novel cell-vertex based finite volume scheme, as there is no reliance on user defined numerical damping to stabilize the scheme [11].

3.1. Ni's Multigrid Method

The explicit multigrid time stepping method used here, involves cycling the solution in a hierarchy of fine and coarse grids, was developed by Ni [9] to accelerate the convergence of his own cell-vertex based finite volume time integration scheme while solving for the nonlinear Euler equations of gas dynamics. Additionaly cell vertex based multigrid method for the Navier-Stokes equations of fluid mechanics are discussed in the Ref. [16, 17]. In this multilevel solution methodology proposed by Ni the basic cell-vertex based finite volume method, also used here, and the multigrid method are strongly coupled. For the basic finite volume scheme the approximation of the flux balance for a computational cell is obtained by evaluating the conservation law in integral form [9]. This solution technique starts with the calculation of "change" in a control volume based on cell vertex flux values. This change is used to determine the "corrections" to be distributed to relevant cell vertices in order to update the state vector (at cell vertices) with the help of relevant distribution formulas [9]. The multigrid technique interwoven with the basic time integration technique employs progressively coarser grids to propagate the fine grid correction rapidly in the computational domain. When this time stepping procedure is applied on the coarse levels, the change for the coarse mesh cells are estimated as the weighted average of the corrections of the fine mesh nodes defining the corresponding coarse mesh cell. These coarse cell changes are distributed to the corners of the coarse mesh cells by the same distribution formula. This procedure is repeated for several coarse levels. Once the coarsest grid reached, the coarser grid correction are then interpolated back on the fine grid and added to the solution of the fine grid. The multigrid process is described below in more detail.

3.1.1. Fine Grid Solution

As mentioned, the fine grid solution in the present work is Ni's cell-vertex based finite volume integration scheme based on the Lax-Wendroff technique. This is briefly described here for the sake of completion. The Lax-Wendroff update for $\mathbf{u}$ is based on a second

order Taylor series approximation

$$\delta\mathbf{u} = \left(\frac{\partial \mathbf{u}}{\partial t}\right)^n \Delta t + \left(\frac{\partial}{\partial t}\left(\frac{\partial \mathbf{u}}{\partial t}\right)\right)^n \frac{\Delta t^2}{2}$$

In above equation, time derivatives can be expressed as space derivatives using Equation (4),

$$\delta\mathbf{u} = -\left(\frac{\partial \mathbf{f}}{\partial x}+\frac{\partial \mathbf{g}}{\partial y}\right)^n \Delta t + \left[\frac{\partial \mathbf{f}}{\partial \mathbf{u}}\frac{\partial}{\partial x}\left(\frac{\partial \mathbf{f}}{\partial x}+\frac{\partial \mathbf{g}}{\partial y}\right)+\frac{\partial \mathbf{g}}{\partial \mathbf{u}}\frac{\partial}{\partial y}\left(\frac{\partial \mathbf{f}}{\partial x}+\frac{\partial \mathbf{g}}{\partial y}\right)\right]^n \frac{\Delta t^2}{2}. \quad (6)$$

Equation (6) is approximated using a cell-vertex based finite volume formulation. Consider a 2-D discretization as shown in Fig. 1, with four cells A, B, C and D and their corresponding vertices where the state vector is defined. The vertices of cell C are marked as 1, 2, 3 and 4. The first order discrete numerical "change" $\Delta\mathbf{U}$ for a arbitrary quadrilateral cell C is approximated using the divergence theorem as

$$\Delta\mathbf{U}_c = \frac{\Delta t}{\Delta\mathcal{A}_c}\left(\sum_{p=1}^{4}\left[\left(\mathbf{F}\left(\mathbf{u}^s\right)\cdot\hat{\mathbf{n}}s\right)_p\right]\right), \quad (7)$$

where $\Delta\mathcal{A}_c$ is the area of the cell C, s the face length with an outer unit normal vector $\hat{\mathbf{n}}$, Δt is the time step restricted by the Courant-Friedrich-Lewy (CFL) stability criteria. Flux vectors $\mathbf{F}(\mathbf{u})$, $\mathbf{G}(\mathbf{u})$ are computed for each pth cell face by taking average of the flux vectors stored at vertices of the face. $\Delta\mathbf{U}_c$ is used for the discrete approximation of the first-order term in Equation (6). The unsteady fluxes [9] $\Delta\mathbf{F}_c$ and $\Delta\mathbf{G}_c$, in the Cartesian x and y directions are defined for each cell as

$$\Delta\mathbf{F}_c = \left(\frac{\partial \mathbf{f}}{\partial \mathbf{u}}\right)\Delta\mathbf{U}_c, \quad \Delta\mathbf{G}_c = \left(\frac{\partial \mathbf{g}}{\partial \mathbf{u}}\right)\Delta\mathbf{U}_c.$$

The second-order changes are based on replacing $(\partial\mathbf{u}/\partial t)$ by $(\Delta\mathbf{U}_c/\Delta t)$ and computed cell wise by an application of the divergence theorem to cell based unsteady flux values $\Delta\mathbf{F}_c$ and $\Delta\mathbf{G}_c$. The components that make up the second-order changes are written as

$$\begin{aligned}\Delta\mathbf{f}_c &= \frac{\Delta t}{\Delta\mathcal{A}_c}\left(\Delta\mathbf{F}_c\Delta y^l + \Delta\mathbf{G}_c\Delta x^l\right)\\ \Delta\mathbf{g}_c &= \frac{\Delta t}{\Delta\mathcal{A}_c}\left(\Delta\mathbf{F}_c\Delta y^m + \Delta\mathbf{G}_c\Delta x^m\right)\end{aligned} \quad (8)$$

where Δx^l, Δy^l, Δx^m and Δy^m are given as [9, 11, 18]. These cell wise changes are appropriately distributed to cell vertices that make up the

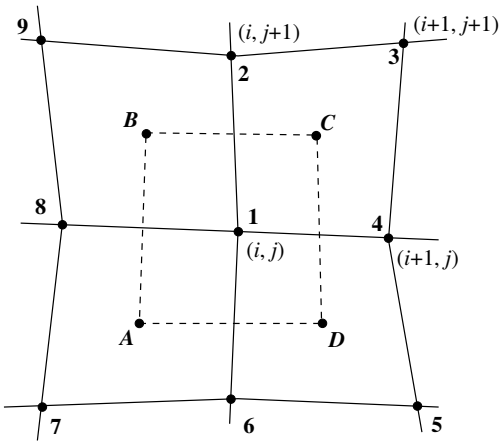

Figure 1. 2-D arbitrary computational cell.

cell using distribution formulas [9]

$$
\begin{aligned}
(\delta \mathbf{u}_1)_c &= \frac{1}{4}\Big[\Delta \mathbf{U}_c - \Delta \mathbf{f}_c - \Delta \mathbf{g}_c\Big] \\
(\delta \mathbf{u}_2)_c &= \frac{1}{4}\Big[\Delta \mathbf{U}_c - \Delta \mathbf{f}_c + \Delta \mathbf{g}_c\Big] \\
(\delta \mathbf{u}_3)_c &= \frac{1}{4}\Big[\Delta \mathbf{U}_c + \Delta \mathbf{f}_c + \Delta \mathbf{g}_c\Big] \\
(\delta \mathbf{u}_4)_c &= \frac{1}{4}\Big[\Delta \mathbf{U}_c + \Delta \mathbf{f}_c - \Delta \mathbf{g}_c\Big].
\end{aligned}
\tag{9}
$$

The total correction at grid point 1, $\delta \mathbf{u}_1$, is obtained by adding the contribution from all four neighboring cells sharing vertex 1

$$
(\delta \mathbf{u}_h)_1 = (\delta \mathbf{u}_1)_a + (\delta \mathbf{u}_1)_b + (\delta \mathbf{u}_1)_c + (\delta \mathbf{u}_1)_d \tag{10}
$$

where, $(\delta \mathbf{u}_1)_a$, $(\delta \mathbf{u}_1)_b$, $(\delta \mathbf{u}_1)_c$, and $(\delta \mathbf{u}_1)_d$ are the contribution of the numerical changes from cells A, B, C and D respectively. The fine grid solution $\mathbf{u}_1^{n+1}$ is updated by adding the fine grid correction $\delta \mathbf{u}_1^n$ to the flow variable at previous time level n. More details are available in Ref. [11].

3.1.2. Coarse Grid Computations

Fine grid corrections calculated using the basic finite volume integration scheme are propagated over a computational domain through successively coarser grids. Successive coarse-grids (Ω_{2h}, Ω_{4h}) are obtained from the previous fine mesh by deleting every alternate

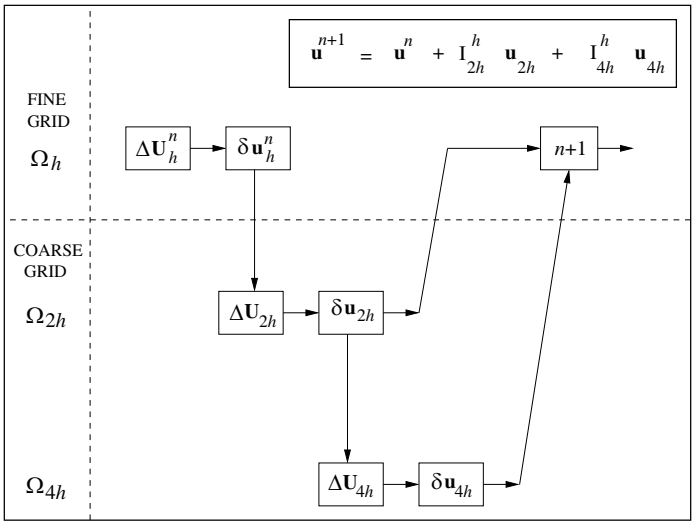

Figure 2. Schematic of multigrid process.

grid line. Consider a mesh Ω_{2h} obtained by deleting alternate grid lines from the fine mesh Ω_h. The "change" in the coarse mesh cell $\Delta\mathbf{U}_{2h}$ is calculated as

$$\Delta\mathbf{U}_{2h} = R_h^{2h}\delta\mathbf{u}_h, \tag{11}$$

where, R_h^{2h} indicates the restriction operator. In the present work, the area weighted average of fine grid corrections is used as a restriction operator. The coarse grid $(2h)$ corrections are calculated using the same distribution formulas used in the basic scheme. This procedure is repeated for several coarse levels. Once the coarsest grid level reached, the coarse corrections are then interpolated back on the fine grid. The state vector $\mathbf{u}$ at next time level are updated by adding each coarse grid correction to the state vector values at previous time level. For a three level multigrid process, the updated value of the state vector $\mathbf{u}$ at time level $n+1$ is given as [9]

$$\mathbf{u}_h^{n+1} = \mathbf{u}_h^n + I_{2h}^h\delta\mathbf{u}_{2h} + I_{4h}^h\delta\mathbf{u}_{4h}, \tag{12}$$

where I_{2h}^h and I_{4h}^h are bilinear interpolation operators in 2D which interpolates the corresponding coarse grid corrections to give the corrections at each grid point on the fine grid. The multigrid process is shown schematically in Fig. 2. Thus, the fine grid corrections are rapidly distributed in the domain. In this method, fine grid corrections are transferred as coarse grid changes. Second order terms in the coarse grid can be described purely in terms of the first order changes in

linear systems as the Jacobian matrix required in defining unsteady flux terms are constants. This is in contrast to that for nonlinear system where the Jacobian matrix on the coarse grids requires to be approximated using fine grid values. This approximation can lead to loss in time accuracy in nonlinear problems as the state vector on the fine grid is retarded in time when compared to the coarse grid.

Time accuracy is particularly important for FVTD solution of the time domain Maxwell's equations in a scattered field formulation. Perfect electric conductor (PEC) boundary conditions are based on the total electric field vector **E** and satisfying this on coarse level requires a time accurate coarse grid solution (scattered field) to synchronize with the analytically available incident field. Time accuracy on coarse levels is not respected in the original Ni's multilevel scheme and is better addressed in Hall's [15] modification of Ni's method described below which is adapted in the present work for the multigrid solution of time domain Maxwell's equations.

3.2. Hall's Extension

Hall [15] developed a cell-vertex multigrid scheme which essentially is a variation of Ni's method. Halls major contribution was to fill in the practical details missing from Ni's [9] original paper.

3.2.1. Fine Grid Solution

The first order change in fine grid at grid point 1 is obtained as a area weighted quantity

$$(\Delta \mathbf{U}_h^n)_1 = \frac{\Delta \mathbf{U}_a \Delta \mathcal{A}_a + \Delta \mathbf{U}_b \Delta \mathcal{A}_b + \Delta \mathbf{U}_c \Delta \mathcal{A}_c + \Delta \mathbf{U}_d \Delta \mathcal{A}_d}{\Delta \mathcal{A}_a + \Delta \mathcal{A}_b + \Delta \mathcal{A}_c + \Delta \mathcal{A}_d} \tag{13}$$

$\Delta\mathcal{A}_a$, $\Delta\mathcal{A}_b$, $\Delta\mathcal{A}_c$, $\Delta\mathcal{A}_d$ are the area for cells A, B, C and D respectively. For a uniform rectangular grid the above expression reduces to Ni's formulation. Unsteady fluxes $\Delta\mathbf{F}_c$ and $\Delta\mathbf{G}_c$ in cell C are found by evaluating the Jacobians at the corresponding vertices as [15]

$$\Delta \mathbf{F}_c = \frac{1}{4}\left[\left(\frac{\partial \mathbf{f}}{\partial \mathbf{u}}\right)_1 + \left(\frac{\partial \mathbf{f}}{\partial \mathbf{u}}\right)_2 + \left(\frac{\partial \mathbf{f}}{\partial \mathbf{u}}\right)_3 + \left(\frac{\partial \mathbf{f}}{\partial \mathbf{u}}\right)_4\right] \Delta \mathbf{U}_c, \tag{14}$$

$$\Delta \mathbf{G}_c = \frac{1}{4}\left[\left(\frac{\partial \mathbf{g}}{\partial \mathbf{u}}\right)_1 + \left(\frac{\partial \mathbf{g}}{\partial \mathbf{u}}\right)_2 + \left(\frac{\partial \mathbf{g}}{\partial \mathbf{u}}\right)_3 + \left(\frac{\partial \mathbf{g}}{\partial \mathbf{u}}\right)_4\right] \Delta \mathbf{U}_c. \tag{15}$$

The total correction at grid point 1, $\delta\mathbf{u}_1$, is obtained by adding the first-order and second-order change contributions as

$$(\delta\mathbf{u}_h)_1 = \Delta\mathbf{U}_1^n + \Bigg[\Big(\Delta\mathbf{F}_b - \Delta\mathbf{F}_d\Big)\Delta y_2 + \Big(\Delta\mathbf{F}_a - \Delta\mathbf{F}_c\Big)\Delta y_1 + \Big(\Delta\mathbf{G}_d - \Delta\mathbf{G}_b\Big)\Delta x_2 + \Big(\Delta\mathbf{G}_c - \Delta\mathbf{G}_a\Big)\Delta x_1\Bigg]\frac{\Delta t}{4\Delta\mathcal{A}_1} \quad (16)$$

where, $\Delta x_1 = (x_b - x_d)$, $\Delta x_2 = (x_c - x_a)$, $\Delta y_1 = (y_b - y_d)$ and $\Delta y_2 = (y_c - y_a)$. The state vector at next time level is updated by adding the total correction $\delta\mathbf{u}_1$ to the state vector at time level n.

3.2.2. Coarse Grid Computations

To advance the solution on coarse grid, the fine grid corrections are restricted on the coarse grids. The first-order change in coarse mesh cell (with centroid 1) is given as [15]

$$(\Delta\mathbf{U}_{2h})_1 = \left(\frac{\delta\mathbf{u}_a^n\mathcal{A}_a + \delta\mathbf{u}_b^n\mathcal{A}_b + \delta\mathbf{u}_c^n\mathcal{A}_c + \delta\mathbf{u}_d^n\mathcal{A}_d}{\mathcal{A}_a + \mathcal{A}_b + \mathcal{A}_c + \mathcal{A}_d}\right)\frac{\Delta t_{2h}}{\Delta t_h^n} \quad (17)$$

where,

$$\delta\mathbf{u}_c^n = \frac{1}{4}\big(\delta\mathbf{u}_1^n + \delta\mathbf{u}_2^n + \delta\mathbf{u}_3^n + \delta\mathbf{u}_4^n\big)$$

and the coarse-grid calculation involves an advance in time through Δt_{2h}. Here, the first order change on coarse grid $\Delta\mathbf{U}_{2h}$, is expressed using weighted average of fine grid corrections at level n, Δt_h^n the fine grid time-step and Δt_{2h}. The correction on the coarse grid is

$$\delta\mathbf{u}_{2h} = \delta\mathbf{u}_h^n\frac{\Delta t_{2h}}{\Delta t_h^n} - \frac{1}{2}\left[\frac{\partial}{\partial x}\left(\frac{\partial\mathbf{f}}{\partial\mathbf{u}}\delta\mathbf{u}_h\right) + \frac{\partial}{\partial y}\left(\frac{\partial\mathbf{g}}{\partial\mathbf{u}}\delta\mathbf{u}_h\right)\right]^n \times (\Delta t_{2h} + \Delta t_h^n) \times \frac{\Delta t_{2h}}{\Delta t_h^n}. \quad (18)$$

This expression for $\delta\mathbf{u}_{2h}$ is a coarse grid but fine-grid accurate representation of $\delta\mathbf{u}_h^{n+1} = \mathbf{u}_h^{n+1} - \mathbf{u}_h^n$ with $\Delta t_{2h} = t^{n+1} - t^n$ obtained by a Taylor series expression around $\mathbf{u}$ [15]. Thus, unlike Ni's original multigrid method time accuracy is attempted to be maintained on the coarse grid. The second order change on coarse mesh cell is obtained in Equation (18) by substituting $\Delta\mathbf{F} \cong (\partial\mathbf{f}/\partial\mathbf{u})\delta\mathbf{u}$ and $\Delta\mathbf{G} \cong (\partial\mathbf{g}/\partial\mathbf{u})\delta\mathbf{u}$, and applying Gauss theorem. Total correction

at grid point 1 is given as [15]

$$\delta\mathbf{u}_{2h}=\Delta\mathbf{U}_{2h}+\Bigg[\Big(\Delta\mathbf{F}_9-\Delta\mathbf{F}_5\Big)\Delta y_2+\Big(\Delta\mathbf{F}_7-\Delta\mathbf{F}_3\Big)\Delta y_1+\Big(\Delta\mathbf{G}_5-\Delta\mathbf{G}_9\Big)\Delta x_2 + \Big(\Delta\mathbf{G}_3-\Delta\mathbf{G}_7\Big)\Delta x_1\Bigg]\frac{\Delta t_{2h}}{\Delta t_h^n}\left(\frac{\Delta t_{2h}+\Delta t_h^n}{4\Delta A_1}\right) \tag{19}$$

where $\Delta x_1 = (x_9 - x_5)$, $\Delta x_2 = (x_3 - x_7)$, $\Delta y_1 = (y_9 - y_5)$ and $\Delta y_2 = (y_3 - y_7)$, ΔA_1 the area of the coarse grid cell 7935. The coarse grid correction are then interpolated back on the fine grid using bilinear interpolation and added to the solution of the fine grid at previous time level.

4. RESULTS

Multigrid results using two and three levels are compared with single (fine) grid solutions. Results are presented for electromagnetic scattering from perfectly electric conductors (PEC) circular cylinder and PEC NACA 0012 airfoil subject to incident harmonic transverse magnetic (TM) wave. Bistatic RCS results are presented for a circular cylinder with $a/\lambda = 9.6$ and $a/\lambda = 14.4$, where a is the radius of cylinder and λ the wavelength of the incident harmonic wave. An 'O' topology grid is used similar to that in Ref. [11], and shown in schematic form in Fig. 3. Initially computations are carried out using a two-level multigrid scheme with a resolution of 10 points per wavelength (PPW) at the scatterer surface on the fine grid and 5 PPW on the coarse grid. The bistatic RCS computed using present multigrid method on two levels is compared with the exact solution, fine grid results and good agreement can be seen in Fig. 4. It may be noted

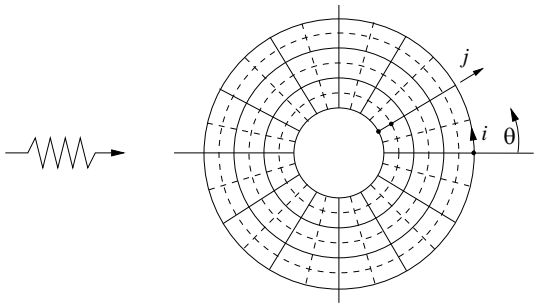

Figure 3. Schematic of grid around circular cylinder.

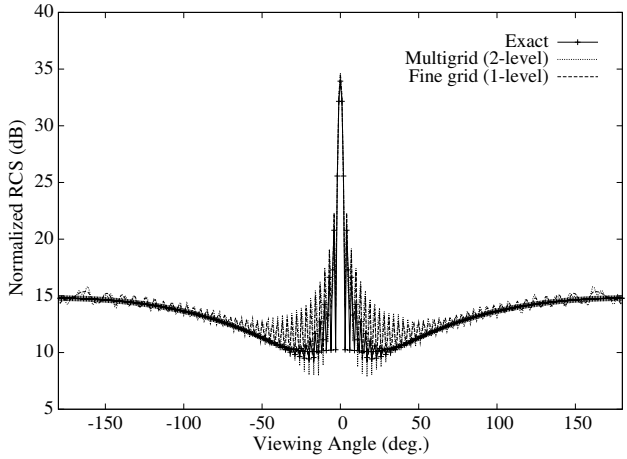

Figure 4. Bistatic RCS, circular cylinder (2 level, $a/\lambda = 9.6$).

Table 1. Multigrid test case description.

Test Case	a/λ	Discretization $(i \times j)$	Grid level
PEC Circular cylinder	9.6	600×50	1
		300×25	2
	14.4	1600×80	1
		800×40	2
		400×20	3
		2000×50	1
		1000×25	2
PEC NACA 0012 Airfoil	10.0	1548×48	1
		774×24	2
		387×12	3

that the dispersion error in the predominantly shadow region is almost identical in both the computed results. This error will reduce with grid refinement as was shown in Ref. [11]. The two-level multigrid method is next used to compute for electromagnetic scattering from a PEC circular cylinder ($a/\lambda = 14.4$). Fine grid discretization with an resolution of 22 PPW is used on the scatterer surface. The two-level

and fine grid results are compared with the exact solution and again good agreement can be seen in Fig. 5. Computations are similarly carried out for a circular cylinder ($a/\lambda = 9.6$) using a three-level multigrid scheme with grid resolution of 26.7 PPW at the finest level on the scatterer surface. Fig. 6 shows a comparison of three-level multigrid and fine grid solution with the exact result. Almost fine-grid accuracy is obtained except for a narrow region in the shadow area between $\pm 50^\circ$. Bistatic RCS obtained using three-level multigrid method, is further compared with a single-level solution on purely the coarsest grid with resolution of 6.67 PPW on scatterer surface. This comparison is done to bring out the ability of the present multigrid method to enforce almost fine grid accuracy while cycling the solution through a hierarchy of grids. This comparison in, Fig. 7, shows the enhanced accuracy of the three-level multigrid solution when compared to a solution obtained on purely the coarsest grid. The coarse grid solution deviates from the exact solution even at the important monostatic point $\pm 180^\circ$. Results are similarly presented for a NACA 0012 airfoil subject to broadside incidence shown in Fig. 8. Bistatic RCS for a TM illumination using three-level multigrid method is compared with fine grid solution and Ref. [19] results in Fig. 9. For this test case an 'O' topology grid is used with finest grid resolution of 24.7 PPW on the scatterer surface and $a/\lambda = 10$, where a indicates the airfoil chord length. Table 2 compares the CPU time used for numerical solution using the multigrid method to that for the purely fine grid solution. For all the cases presented, a reduction of CPU time between

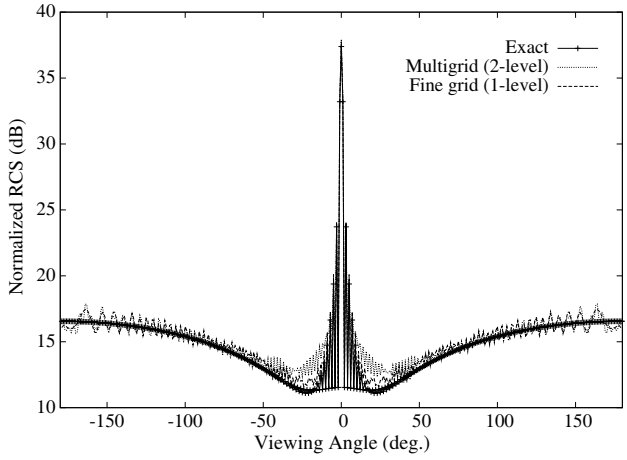

Figure 5. Bistatic RCS, circular cylinder (2 level, $a/\lambda = 14.4$).

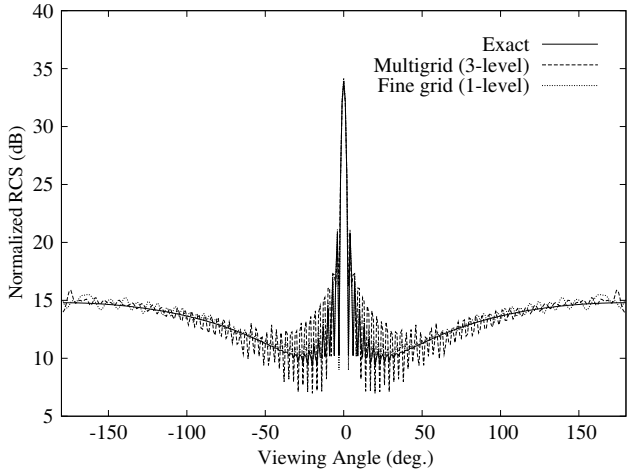

Figure 6. Bistatic RCS, circular cylinder (3 level, $a/\lambda = 9.6$).

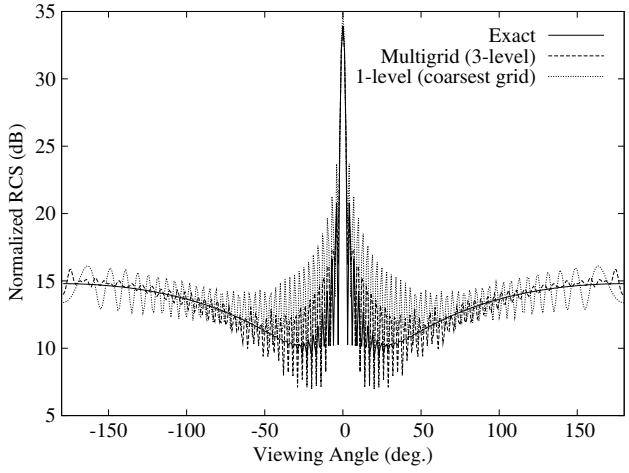

Figure 7. Bistatic RCS, circular cylinder (3 level and coarsest grid, $a/\lambda = 9.6$).

30 and 40% is obtained. Reduction in CPU time is obtained due to the larger time steps allowed on coarser levels due to the relaxed stability criteria arising out of increased cell sizes. The larger time-step allowed on coarser level means more rapid wave movement on coarser levels leading to faster convergence. The number of grid points also reduce with successive coarsening resulting in less computational

effort. Overheads during the multigrid process include restricting fine grid variables on the coarse grid as well as interpolating corrections to the fine grid. There is no significant increase in memory requirement in the multigrid process since coarse-grid corrections are not required to be stored at each level and can be transferred immediately to the fine grid. Each multigrid cycle consist of one iteration on each level and typically 1000 such cycles are required for convergence to a time-harmonic steady state. The number of levels in the multigrid method are limited by the minimum discretization available on the coarsest level. Numerical experiments indicate a minimum resolution of 5–6 PPW on the scatterer surface at the coarsest level requires to be adhered to for obtaining almost fine-grid accuracy in the multigrid process. No additional numerical damping was required to stabilize the multigrid method or to smoothen out interpolation errors which are essential while solving for nonlinear hyperbolic problems like Euler's equations of gas dynamics.

Table 2. CPU times (seconds).

Test Case	a/λ	Grid levels	CPU Time (s)		% saving in CPU time
			Basic scheme (fine grid)	multigrid	
Circular cylinder	9.6	2	126.24	79.53	37
Circular cylinder	14.4	2	408.7	289.68	29
Circular cylinder	9.6	3	1820	1073	41
NACA 0012 airfoil	10.0	3	224.49	152.65	32

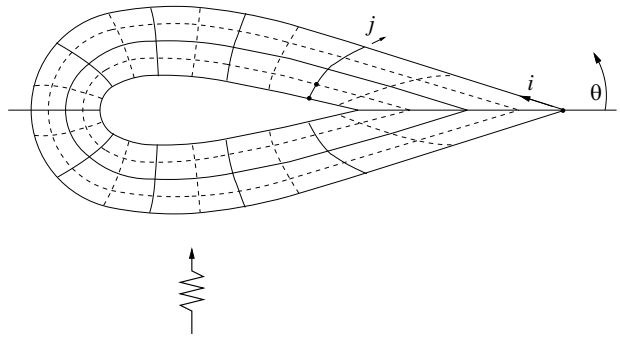

Figure 8. Schematic of grid around NACA 0012 airfoil.

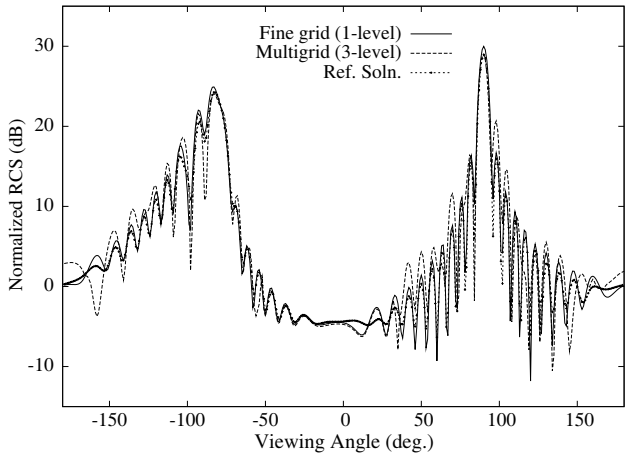

Figure 9. Scattering from a NACA 0012 using multigrid (3 grid, $a/\lambda = 10$).

5. CONCLUSION

The time domain Maxwell's equations posed as a set of hyperbolic conservation laws are solved using a cell-vertex based multilevel scheme originally proposed by Ni for the solution of nonlinear Euler equations of gas dynamics. Unlike solution of Euler equations, the linear Maxwell's system does not requires the Jacobian to be approximated on coarser levels leading to the better implementation. Hall's modification of original Ni's scheme allows time synchronization of incident and scattered field on coarser levels due to time accuracy of the transient solution on the coarse grid. No artificial damping is required to stabilize the multigrid technique for the linear Maxwell's system or to dampen interpolation errors. The reduction in CPU time along with almost fine-grid accuracy of the obtained multigrid solution suggests that this technique could be useful in more practical three-dimensional applications involving electromagnetic scattering.

REFERENCES

1. Shankar, V., "A gigaflop performance algorithm for solving Maxwell's equations of electromagnetics," *AIAA Paper*, 584–590, 91–1578, June 1991.
2. Chatterjee, A. and R. S. Myong, "Efficient implementation of higher-order finite volume time-domain method for electrically

large scatterers," *Progress In Electromagnetics Research B*, Vol. 17, 233–254, 2009.

3. Shang, J. S., "Characteristic-based algorithms for solving the Maxwell equations in the time domain," *IEEE Antennas and Propagation Society Magazine*, Vol. 37, No. 3, 15–25, 1995.
4. Chatterjee, A. and A. Shrimal, "Essentially nonoscillatory finite volume scheme for electromagnetic scattering by thin dielectric coatings," *AIAA Journal*, Vol. 42, No. 2, 361–365, 2004.
5. Yee, K., "Numerical solutions of initial boundary value problems involving Maxwell's equations in isotropic media," *IEEE Transactions on Antennas and Propagation*, Vol. 14, 302–307, 1966.
6. Brandt, A., "Multi-level adaptive solutions to boundary-value problems," *Mathematics of Computation*, Vol. 31, No. 138, 333–390, 1977.
7. Turkel, E., "Progress in computational physics," *Computers and Fluids*, Vol. 11, No. 2, 121–144, 1983.
8. Chatterjee, A. and G. Shevare, "A time-accurate multigrid algorithm for Euler equations," *Fourteenth International Conference on Numerical Methods in Fluid Dynamics*, Lecture Notes in Physics, 453, Springer-Verlag, 1995.
9. Ni, R.-H., "A multiple-grid scheme for solving the Euler equations," *AIAA Journal*, Vol. 20, 1565–1571, 1982.
10. Jameson, A., "Solution of the Euler equations for two-dimensional flow by a multigrid methods," *Applied Mathematics and Computation*, Vol. 13, 327–356, 1983.
11. Deore, N. and A. Chatterjee, "A cell-vertex finite volume time domain method for electromagnetic scattering," *Progress In Electromagnetics Research M*, Vol. 12, 1–15, 2010.
12. Koeck, C., "Computation of three-dimensional flow using the Euler equations and a multiple-grid scheme," *International Journal for Numerical Methods in Fluids*, Vol. 5, 483–500, 1985.
13. Ni, R. H. and J. C. Bogoian, "Prediction of 3-D multistage turbine flow field using a multiple-grid Euler solver," *AIAA Paper*, 1–9, 89–0203, Jan. 1989.
14. Roe, P. L., "Fluctuations and signals — A framework for numerical evolution problems," *Numerical Methods in Fluid Dynamics*, K. W. Morton and M. J. Baines (eds.), 219–257, Academic Press, 1982.
15. Hall, M. G., "Cell-vertex multigrid schemes for solution of the Euler equations," *Numerical Methods for Fluid Dynamics II*,

K. W. Morton and M. J. Baines (eds.), 303–345, Clarendon Press, Oxford, 1985.

16. Radespiel, R., C. Rossow, and R. C. Swanson, "Efficient cell-vertex multigrid scheme for the three-dimensional Navier-Stokes equations," *AIAA Journal*, Vol. 28, No. 8, 1464–1472, 1990.
17. Swanson, R. C. and R. Radespiel, "Cell centered and cell vertex multigrid schemes for the Navier-Stokes equations," *AIAA Journal*, Vol. 29, No. 5, 697–703, 1991.
18. French, A. D., "Solution of the Euler equations on cartesian grids," *Applied Numerical Mathematics*, Vol. 49, 367–379, 2004.
19. Shankar, V., W. F. Hall, and A. H. Mohammadin, "A time-domain differential solver for electromagnetic scattering problems," *Proceedings of the IEEE*, Vol. 77, No. 5, 709–721, 1989.